Title 論文題目	An enriched environment improves diabetes-induced cognitive impairment by enhancing exosomal miR-146a secretion from endogenous bone marrow-derived mesenchymal stem cells (刺激豊かな環境が内因性骨髄由来間葉系幹細胞が分泌するエクソソームに含まれる miR-146a を増加させることにより糖尿病由来の認知症を改善する)
Author(s) 著　者	久保田, 健太
Degree number 学位記番号	甲第 2963 号
Degree name 学位の種別	博士（医学）
Issue Date 学位取得年月日	2017-03-31
Original Article 原著論文	札幌医学雑誌　第 86 巻 1 号（平成 30 年 3 月）
Doc URL	
DOI	
Resource Version	

An enriched environment improves diabetes-induced cognitive impairment by enhancing exosomal miR-146a secretion from endogenous bone marrow-derived mesenchymal stem cells

Kenta Kubota[1,3], Masako Nakano[1], Eiji Kobayashi[1], Yuka Mizue[1,2], Takako Chikenji[1,2], Miho Otani[2], Kanna Nagaishi[1,2], Mineko Fujimiya[1,2]*

[1]Department of Anatomy, and [2]Department of Diabetic Cellular Therapeutics, Sapporo Medical University, School of Medicine, Sapporo, Hokkaido, 060-8556, Japan. [3]Department of Physical Therapy, Hokkaido Chitose Rehabilitation University, Chitose, Hokkaido, 066-0055, Japan.

E-mail addresses

Kenta Kubota : k-kubota@sapmed.ac.jp

Masako Nakano : m.nakano@sapmed.ac.jp

Eiji Kobayashi : ekobayashi@sapmed.ac.jp

Yuka Mizue : y-mizue@sapmed.ac.jp

Takako Chikenji : chikenji@sapmed.ac.jp

Miho Otani : motani@sapmed.ac.jp

Kanna Nagaishi : kanna@sapmed.ac.jp

＊Mineko Fujimiya : fujimiya@sapmed.ac.jp

Abstract

Increasing evidence suggests that enriched environments (EEs) ameliorate cognitive impairment by promoting the repair of brain damage. However, the mechanisms by which this occurs have not been determined. To address this issue, we investigated whether EEs enhance the capability of endogenous bone-marrow derived mesenchymal stem/stromal cells (BM-MSCs) to repair diabetic hippocampal damage by focusing on miRNA carried in BM-MSC derived exosomes. In diabetic STZ rats housed in an EE (STZ/EE), cognitive impairment was significantly reduced and hippocampal damage was repaired compared with STZ rats housed in conventional cages (STZ/CC). BM-MSCs isolated from STZ/CC rats had functional and morphological abnormalities that were not detected in STZ/EE BM-MSCs. Intravenous injection of BM-MSCs from STZ/CC rats into diabetic mice had no effect, while injection of BM-MSCs from STZ/EE rats reversed cognitive impairment and helped repair hippocampal damage. The analysis of exosomal miR-146a levels in conditioned medium from cultured BM-MSCs, sera from mice intravenously injected with BM-MSCs from STZ/CC or STZ/EE rats, and sera from Control/CC, STZ/CC and STZ/EE rats, suggested that EEs stimulate up-regulation of exosomal miR-146a secretion by endogenous BM-MSCs, which exerts anti-inflammatory effects on damaged astrocytes and ameliorates diabetes-induced cognitive impairment.

Introduction

Cognitive impairment associated with diabetes is a worldwide problem, and diabetes increases the risk of dementia 2-3 fold[1]. Hyperglycemia induces brain damage by increasing arteriosclerosis, oxidative stress and insulin resistance in the central nervous system (CNS)[2]. In type 1 diabetic rodent models, various abnormalities have been noted, including aberrant neuronal activities, decreased synaptic plasticity, and astroglial damage in the hippocampus[3,4]. In Type 2 diabetic rodent models, reduced insulin signaling and metabolic disturbance, in addition to neuronal and astroglial abnormalities in the hippocampus, have been reported[5,6].

Cognitive rehabilitation is widely used as a non-pharmacological intervention for patients with cognitive impairments caused by diabetes, Alzheimer's disease or Parkinson's disease[7]. However, the mechanisms that lead to memory and psychological improvement have not been fully clarified[8]. To elucidate how environmental stimulation affects cognitive impairment, we investigated the effectiveness of enriched environment (EEs) for improving cognitive impairment caused by diabetes in rodents.

EEs are those in which animals have frequent opportunities for social interaction and physical activity compared with conventional cages[9]. In EEs, animals are kept in large groups in a spacious cage with running wheels, toys and mazes that are moved frequently[9]. In rodents, EEs have been reported to provide beneficial effects for neurodegenerative disorders such as Alzheimer's disease and Parkinson's disease[10,11]. EEs induce experience-dependent plasticity[12], promote neurogenesis[13],

increase the expression of neurotransmitters and trophic factors including BDNF[14-16], enhance the density of dendritic spines[17], and drive epigenetic changes[18]. EEs stimulate circulating immune cells to secrete anti-inflammatory exosomic microRNAs (miRNAs), which may be effective against demyelinating disease in the CNS[19]. In diabetic models, it has been reported that EEs increase neurogenesis in the hippocampus and the density of dendrites and spines via experience-dependent plasticity[13,20,21]. Although evidence is accumulating that EEs improve cognitive impairment by promoting brain damage repair, no previous studies have demonstrated a relationship between EE enhanced brain functions and functional roles of bone-marrow derived mesenchymal stem/stromal cells (BM-MSCs).

Recently we showed that systemic injection of BM-MSCs ameliorated diabetes-induced cognitive impairment, and confirmed that exosomes derived from BM-MSCs are involved in the repair of damaged astrocytes and neurons in a type 1 diabetic model[22]. BM-MSCs are a powerful tool for combatting various disorders, including hepatic dysfunction[23], nephropathy[24], and wound healing[25], by suppressing inflammation and repairing damaged organs[26], while BM-MSCs isolated from diabetic animal do not exert enough therapeutic function[27]. Exosomes, which are extracellular vesicles containing mRNAs, miRNAs and proteins, are released from BM-MSCs and transported to target cells to influence recipient cell function[28]. For example, exosomes derived from BM-MSCs promote angiogenesis in acute myocardial infarction in rats[29], improve renal function[30], and enhance functional recovery in a stroke model via miR-133b transfer into neurons and astrocytes[31]. Since our

previous study showed that BM-MSCs can improve diabetes-induced cognitive impairment by secreting exosomes[22], we hypothesized that EEs activate the endogenous BM-MSC and exosomes derived from activated BM-MSCs can ameliorate neuronal and astroglial damage in diabetic models.

In this study we investigated whether EEs enhance the capability of endogenous BM-MSCs to repair hippocampal damage caused by diabetes by focusing on miRNA carried in BM-MSC derived exosomes.

Results

An EE prevents learning and memory impairment in diabetic rats

Control/CC and STZ/CC rats were housed in control cages (CCs), while STZ/EE rats were housed in EE cages for 8 weeks after STZ or vehicle injection. Subsequently, the animals underwent a series of Morris water maze (MWM) tests and were sacrificed for morphological analysis (Fig. 1a). During the experimental period from 1 to 8 weeks after STZ injection, no differences were observed in the body weights and blood glucose levels of the STZ/CC and STZ/EE groups (Fig. 1b).

In the hidden platform training of the MWM tests, STZ/CC rats took longer to reach the platform than Control/CC rats on days 2, 3 and 4. On the other hand, STZ/EE rats had a shortened escape latency compared with the STZ/CC rats on days 3 and 4 (Fig. 1c). There were no differences in the swimming speeds among the three experimental groups (Control/CC, $0.28 \pm 0.01 ms^{-1}$; STZ/CC, $0.25 \pm 0.01 ms^{-1}$; STZ/EE, $0.23 \pm 0.02 ms^{-1}$). In addition, we found no differences in sensory, motor and motivational aspects between the three groups in the visible platform training sessions. During the probe test, the Control/CC and STZ/EE rats spent significantly longer in the target quadrant (South East, SE) than in other areas (Fig. 1c). In contrast, the time spent by STZ/CC rats in the SE target quadrant was not significantly different from other quadrants.

An EE prevents neuronal loss, decreases oxidative stress and enhances synaptic density

We investigated the mechanisms by which EEs prevent diabetes-induced cognitive

impairment. The number of NeuN-positive cells in the hippocampal CA1 region in STZ/CC rats was significantly lower than in Control/CC rats, while that of STZ/EE rats was significantly higher than STZ/CC rats (Fig. 2a). The staining intensity of the 4-hydroxynonenal (4HNE)-positive area, an oxidative stress marker, was significantly increased in the CA1 region in STZ/CC rats, while the staining intensity in STZ/EE rats was equivalent to Control/CC rats (Fig. 2b). Furthermore, the intensity of synaptophysin staining was significantly decreased in STZ/CC rats, while STZ/EE rats had a significantly higher staining intensity than STZ/CC and Control/CC rats. (Fig. 2c). These results suggest that EEs prevent neuronal loss, decrease oxidative stress and enhance synaptic plasticity in the CA1 region in STZ-diabetic rats.

An EE prevents increases in astroglial inflammation.

When we investigated the effects of EEs on astrocytes by immunohistochemical staining for the astrocyte marker GFAP, there were no significant differences in GFAP positive areas in the CA1 region between the three groups (Fig. 2d). Thus, we performed immunohistochemical overlap staining for GFAP and TNF-α (an inflammatory cytokine), to examine the astrocytes in more detail. Although the TNF-α positive area to GFAP positive area ratio was significantly increased in STZ/CC rats, the ratio in STZ/EE rats was equivalent to levels in Control/CC rats (Fig. 2e). These results suggest that EEs prevent cytokine expression by astrocytes in the CA1 region in diabetic rats.

The EE ameliorates BM-MSC abnormalities in STZ rats

We investigated the characteristics of BM-MSCs in the Control/CC, STZ/CC and STZ/EE groups, focusing on histological findings, and proliferation and migration abilities. Phase-contrast microscopy analysis revealed that the shape of BM-MSCs in STZ/CC rats was flat and broad compared with BM-MSCs in Control/CC rats, which were slim and spindle shaped with long cytoplasmic processes. On the other hand, the shapes of BM-MSCs in STZ/EE rats were similar to those in Control/CC rats (Fig. 3a). The minor axis of the cells, defined as the minimal length passing through the nucleus, was significantly longer in STZ/CC rats, while the length in STZ/EE BM-MSCs was similar to Control/CC rats (Fig. 3a).

Cell growth measured by the MTT proliferation assay was reduced in STZ/CC BM-MSCs compared to Control/CC at 48h and 72h; however, proliferation of STZ/EE BM-MSCs was significantly greater than STZ/CC BM-MSCs at 72h (Fig. 3b). Furthermore, cell mobilization assessed by the scratch assay was down-regulated in STZ/CC BM-MSCs and up-regulated in STZ/EE. Notably, the open wound area was significantly larger in STZ/CC cultures, while the area in STZ/EE cultures was smaller than in STZ/CC cultures at 12h (Fig. 3c). These results suggest that an EE ameliorates BM-MSC abnormalities caused by STZ-diabetes.

Intravenous injection of BM-MSCs isolated from STZ/EE rats ameliorates learning and memory impairments in diabetic mice

Because we previously reported that normal rat BM-MSCs can improve learning and memory impairments in diabetic mice after intravenous injection, we hypothesized that diabetic BM-MSCs with EE mediated enhanced function may have therapeutic potential for the treatment of cognitive impairments caused by diabetes. To examine this hypothesis, we injected BM-MSCs derived from STZ/CC and STZ/EE rats into diabetic mice. Based on our previous study, 1×10^4 BM-MSCs/g body weight were administered intravenously from 12 weeks after STZ injections, 4 times at 2-weeks intervals. The mice then underwent a series of MWM tests and were sacrificed for morphological analysis (Fig. 4a).

At the 20th week after STZ injection, there were no significant differences in body weight and blood glucose levels among the three groups (Fig. 4b). In the MWM hidden platform training, STZ/EE BM-MSC iv mice had a shorter escape latency than Vehicle iv mice and STZ/CC BM-MSC iv mice on day 4 (Fig. 4c). There were no significant differences in the swimming speed among the three groups (Vehicle iv, $0.1 \pm 0.002 ms^{-1}$; STZ/CC BM-MSC iv, $0.093 \pm 0.003 ms^{-1}$; STZ/EE BM-MSC iv, $0.091 \pm 0.001 ms^{-1}$). In addition, we found no significant differences in sensory, motor and motivational aspects in the visible platform training sessions involving the three groups. During the probe test, the time spent in the SE quadrant was not significantly different from other areas when Vehicle iv and STZ/CC BM-MSC iv groups were compared. In contrast, the time spent in the SE quadrant was significantly longer than in other areas in the STZ/EE BM-MSC iv group (Fig. 4c).

Intravenous injection of BM-MSCs isolated from STZ/EE rats does not increase the number of neurons, but decreases oxidative stress and enhances synaptic density

We investigated the mechanisms by which STZ/EE BM-MSCs ameliorate diabetes-induced cognitive impairment. The number of NeuN-positive cells in the CA1 region was not altered among the three groups (Fig. 5a). However, the intensity of 4HNE staining in the CA1 region of STZ/EE BM-MSC iv mice was significantly decreased compared to Vehicle iv or STZ/CC BM-MSC iv mice (Fig. 5b). Furthermore, the intensity of synaptophysin staining in the CA1 region of STZ/EE BM-MSC iv mice was significantly increased compared to Vehicle iv or STZ/CC BM-MSC iv mice (Fig. 5c).

Intravenous injection of BM-MSCs isolated from STZ/EE rats suppresses increases in astroglial inflammation

We investigated the effect of STZ/EE BM-MSCs on astrocytes by immunohistochemical staining of GFAP. There were no significant differences in GFAP positive areas in the CA1 regions among the three groups (Fig. 5d). However, the ratio of TNF-α positive area to GFAP positive area in STZ/EE BM-MSC iv mice was significantly decreased compared to Vehicle iv or STZ/CC BM-MSC iv mice (Fig. 5e).

Increased exosomal miR-146a secretion was observed in the conditioned medium from

cultured STZ/EE BM-MSCs, sera from STZ/EE BM-MSC injected mice and sera from STZ/EE rats

We examined the concentration of exosomal miR-146a in the conditioned medium of cultured BM-MSCs. Firstly, we confirmed the presence of exosomes in conditioned medium from cultured BM-MSCs, and in mouse and rat serum, by assessing the presence of the common exosomal markers CD63 and HSP70 (Fig. 6a). The concentration of miR-146a in exosomes released by STZ/CC BM-MSCs was significantly lower than Control/CC BM-MSCs, while the levels in STZ/EE BM-MSCs were significantly higher than those in STZ/CC BM-MSCs (Fig. 6b). The serum levels of exosomal miR-146a in STZ/EE BM-MSC iv mice were significantly higher than that in Vehicle iv and STZ/CC BM-MSC iv mice (Fig. 6c). The serum levels of exosomal miR-146a in STZ/CC rats were significantly lower than Control/CC, while the serum levels of exosomal miR-146a in STZ/EE rats were significantly higher than those in STZ/CC rats (Fig. 6d).

We also investigated the concentration of miR-181a in BM-MSC conditioned medium. No differences in exosomal miR-181a levels were detected in BM-MSC conditioned media from the three groups (Fig. 6e). Moreover, the serum levels of exosomal miR-181a in STZ/CC rats and STZ/EE rats were significantly decreased compared with those of Control/CC rats (Fig. 6f).

Discussion

To our knowledge this is the first report to show that an EE can activate BM-MSCs and ameliorate cognitive impairment caused by diabetes. We found that an EE inhibits diabetes-induced cognitive impairment even under hyperglycemic conditions, and at the same time ameliorates functional abnormalities of cultured BM-MSCs caused by diabetes. We also found that systemic injection of BM-MSCs activated by an EE has therapeutic potential for the treatment of diabetes-induced cognitive impairment. Finally, we showed that exosomal miR-146a originating from endogenous BM-MSCs might be one of the key molecules up-regulated in response to an EE, and may play a role in minimizing cognitive impairment by reducing inflammation.

We housed diabetic rats in an EE for 8 weeks after STZ injection and then conducted MWM tests to examine learning and memory abilities. STZ/CC rats performed relatively worse in the MWM test; however cognitive function recovered in STZ/EE rats to the level in Control/CC rats. Because no differences were found in the swimming speeds among the three groups, or the body weights and blood glucose levels of the STZ/CC and STZ/EE rats, the results suggest that the prevention of cognitive decline by an EE might not be due to reduced hyperglycemia or sensorimotor deficits.

Recently our group reported that systemic injection of BM-MSCs ameliorated diabetic complications, including nephropathy, hepatic dysfunction, and cognitive impairments without improving hyperglycemia[22-24]. In addition, it was shown that BM-MSCs suppress oxidative stress,

reverse astrocyte abnormality, and facilitate synaptic plasticity in hippocampi damaged by diabetes[22]. BM-MSCs also improve neuronal recovery after stroke by secreting neurotrophic factors, increasing angiogenesis and synaptogenesis, and promoting glial remodeling[32]. In the present study, we found that an EE helps repair hippocampal damage caused by diabetes in a similar way to systemic injection of BM-MSCs[22]. Recently, it was shown that endogenous BM-MSCs stimulated with granulocyte colony stimulating factor (G-CSF) increased the regeneration of damaged inner ear hair cells without injection of exogenous BM-MSCs[33]. Thus, we hypothesized that an EE has the potential to prevent cognitive impairment at least in part by activating endogenous BM-MSCs. On this basis, we aimed to elucidate how an EE influences endogenous BM-MSC function, and how EE-activated BM-MSCs improve cognitive impairment in diabetic animals.

In in vitro culture experiments, STZ/CC BM-MSCs exhibited an abnormal flattened shape with an increased minor axis length, impaired proliferation ability, and decreased migratory potential. These abnormalities were considered to be due to cell senescence caused by diabetes, because it has been shown that diabetes induces BM-MSC senescence by up-regulating autophagy[34] and aging causes the enlargement of BM-MSCs[35]. It is also known that BM-MSC senescence reduces proliferative ability and impairs migration response by activating the p53/p21 pathway and inhibiting the AP-1 pathway[36]. In the present study, the abnormalities in BM-MSCs caused by diabetes were completely prevented in response to an EE. How this occurs is not clear at present. However, it is possible that EEs suppress the hypothalamic-pituitary-adrenal (HPA) axis[20] and the subsequent

reduction in cortisol level, which is linked to cytotoxicity[37], might result in the functional enhancement of endogenous BM-MSCs.

In our previous study, systemic injection of BM-MSCs obtained from normal rats ameliorated cognitive impairment and helped repair hippocampal damage in STZ diabetic mice[22]. With this in mind, we examined the effects of STZ/CC and STZ/EE BM-MSCs on cognitive impairment and hippocampal damage in STZ mice. Based on our previous study[22], we injected STZ/CC BM-MSCs or STZ/EE BM-MSCs into mice 4 times at 2-weeks intervals 12 weeks after STZ injections, at the time animals show cognitive impairment with neuronal loss. STZ/CC BM-MSC injected mice showed impaired performance in the MWM test, while cognitive function was improved in STZ/EE BM-MSC treated mice. Morphological analysis of the hippocampus revealed that STZ/EE BM-MSC injected mice had reduced oxidative stress, increased synaptic density, and down-regulated TNF-α expression in astrocytes. In the present study, the expression of GFAP in astrocytes was not altered in the three groups, while previous reports described increased or decreased expression of GFAP in the brains of diabetic models[38,39]. Therefore, we examined the co-expression of TNF-α and GFAP to evaluate the characteristics of astrocytes, because TNF-α is a useful marker of astrocyte inflammation[40].

Astrocytes play important roles, including supplying lactate to neurons, adjusting extracellular K^+ levels, removing excess glutamate, and promoting synaptogenesis[41,42]. Astrocytes reduce oxidative stress and suppress apoptosis in neurons[43,44]. On the other hand, TNF-α released

from astrocytes is known to generate excessive reactive oxygen species (ROS) and induce neuronal death[45]. We found that even though neuronal loss was sustained in STZ/EE MSC treated mice, cognitive impairment was reduced. This result suggests that synaptogenesis supported by astrocytes is more important for maintaining cognitive function than overall neuronal number[46].

Our results showed that diabetes induces BM-MSC abnormalities that can be reversed by an EE, furthermore EE-enhanced BM-MSCs have the potential to repair cognitive impairment and hippocampal damage caused by diabetes. Since it has been shown that BM-MSCs release exosomes that are taken up by astrocytes and exert neuroprotective functions[22], it is possible EE enhanced BM-MSCs may release exosomes that contain neuroprotective components.

miRNA-146a is known to exert anti-inflammatory effects by suppression of tumor necrosis factor receptor-associated factor 6 (TRAF6) and IL-1 receptor associated kinase 1 (IRAK1)[47]. The astrocyte mediated anti-inflammatory effects of miR-146a have been shown to be associated with the inhibition of IL-6, IL-8, G-CSF, IFN-γ, IP-10, MIP-1b, and TNF-a[48]. However, in diabetes, decreased serum levels of miR-146a correspond to chronic inflammation[49], and miR-146a deficiency leads to diabetic nephropathy by activating macrophages[50]. Hyperglycemia downregulates miR-146a expression in dorsal root ganglia (DRG) neurons, and elevation of miR-146a expression in DRG neurons increases neuronal survival even under high glucose conditions[51]. In addition, BM-MSCs are known to improve diabetic wound healing by increasing the level of miR-146a at the lesion[25], and anti-inflammatory effects of miR-146a derived from umbilical cord MSCs have also been

demonstrated[52].

We examined the concentrations of miR-146a in conditioned BM-MSC media from Control/CC, STZ/CC and STZ/EE rats. The miR-146a level was decreased in STZ/CC BM-MSCs compared with Control/CC BM-MSCs, and STZ/EE BM-MSCs had miR-146a levels similar to controls. This result suggests that the EE prevented the decrease in miR-146a levels in BM-MSC derived exosomes in diabetes which recovered to normal levels. Next, we examined whether the increase in miR-146a levels in EE enhanced cultured BM-MSCs corresponded to miR-146a levels in serum exosomes from mice injected with BM-MSCs from STZ/CC and STZ/EE rats. Mice injected with STZ/EE BM-MSCs had a remarkable increase in serum exosomal miR-146a levels compared with those injected with STZ/CC BM-MSCs, suggesting that miR-146a detected in mouse serum may originate from exogenously injected BM-MSCs. Although various cell types, including immune cells, are known to release miR-146a[53], our results raise the possibility that exosomal miR-146a derived from BM-MSCs may contribute to repair of hippocampal damage caused by diabetes.

To confirm the involvement of exosomal miR-146a derived from endogenous BM-MSC to repair the hippocampal damage, we examined the changes in miR-146a levels in serum exosomes from Control/CC, STZ/CC and STZ/EE rats. We detected a recovery in miR-146a levels in exosomes from STZ/EE rat serum compared with STZ/CC rat serum, suggesting that increased levels of miR-146a in STZ/EE rat serum are possibly derived from endogenous BM-MSC and such increase may contribute to repair of hippocampal damage and subsequently recover the cognitive

impairment.

The involvement of another miRNA, miR-181a, which is known to exert anti-inflammatory effects on astrocytes[54], was also examined. No differences were found in the levels of exosomal miR-181a in the conditioned media of cultured BM-MSCs from STZ/CC and STZ/EE rats, and no differences were found in the serum levels of exosomal miR-181a in STZ/CC and STZ/EE rats, suggesting that miR-181a is not directly involved in EE-induced activation of BM-MSCs.

The increased levels of miR-146a in serum exosomes from EE housed rats may help prevent astrocytic damage by internalizing of exosomes into astrocytes, because it has been shown that BM-MSC derived exosomes are taken up into astrocytes mainly after icv injection[22]. BM-MSC derived exosomes are also transferred to neurons to some extent, therefore miR-146a might have supported neuronal survival in STZ/EE rat. Although many mediators beside miR-146a are secreted by BM-MSCs[55], we consider that miR146a is one of the key factors that influence astrocyte functions and subsequently enhance neuroprotective effects.

Overall, our data indicate that environmental stimulation, including active communication, stress reduction and exercise are important to improve cognitive impairment in diabetic rodents. A deeper understanding of the precise mechanisms by which this occurs may have important ramifications for the development of more effective treatments for human patients with diabetic cognitive impairment.

Methods

Animals

All following experimental methods were conducted in accordance with the approved guidelines. Hyperglycemia was induced in 9-week-old male SD rats (Japan SLC, Shizuoka, Japan) by a single intravenous injection (iv) of streptozotocin (STZ) (55mg/kg; Wako, Osaka, Japan) dissolved in citrate buffer (pH4.5) at 9 weeks of age. After confirming blood glucose levels were above 300 mg/dL, STZ rats were housed in conventional cages (STZ/CC) or enriched environment (STZ/EE) cages for 8 weeks. Control rats (Control/CC) were administered with iv citrate buffer, and housed in conventional cages for 8 weeks. Hyperglycemia was induced in C57BL/6j mice (Japan SLC) by a single ip injection of STZ (150mg/kg) dissolved in citrate buffer (pH4.5) at 13 weeks of age. We used STZ mice with blood glucose levels above 300mg/dL. All experiments were conducted according to the methods approved by the animal experiment committee of Sapporo Medical University.

Housing conditions

During the experimental period, rats were housed in (1) conventional cages (CC, 260mm × 420mm × 200mm) with 2 rats per cage or (2) environmental enrichment cages (EE, 600mm × 800mm × 480mm) with 11 rats per cage and two levels according to a previous report[56]. The first level consisted of 2 running wheels, 1 tunnel, a red rectangular house, and places for food and water

access, while the second level contained the maze (Fig. 1a), which was changed 3 times a week.

Morris water maze (MWM) tests

The MWM test was carried out according to a previous study[22]. Rats and mice were placed in a maze that consisted of a circular pool (1.2m diameter) filled with water (25 ± 1℃). This pool size has been used for both rats and mice in previous reports[57,58]. In this experiment, animals were trained in visible platform sessions (day 0) and then hidden platform sessions were performed 4 times a day with 1h intervals (day 1-4). The platform was in the center of the south-east quadrant and placed 1cm below the surface of the water during the visible and hidden tests. Each trial had a limit of 90 sec, and the time to reach the platform (escape latency) and swim speed were recorded. When animals failed to reach the platform within 90 sec, they were placed on the platform for 15 sec. At day 5, after removing the platform, the probe test was conducted in which the time spent in each quadrant in 90 sec was recorded. An automated tracking system (Any-maze, Stoelting, Wood Dale, IL, USA) was used to record the data.

Immunofluorescence staining

Brains were removed from the skull and fixed in a solution of 4% PFA and 0.2% picric acid in 0.1M phosphate buffer for 24h and then immersed in a 15% sucrose solution. Brains (n = 3-4/group) were cut into 20μm thick frozen sections, and 3 coronal sections of the left hippocampus

(for rats and mice, 2.5-3.5 and 1.5-2.5mm posterior to the bregma, respectively) were chosen for each immunostaining.

The sections were incubated overnight at 4℃ with primary antibodies against NeuN (rabbit polyclonal, 1:1000; Millipore, Darmstadt, Germany), 4-hydroxynonenal (4HNE) (rabbit polyclonal, 1:100; Abcam, Cambridge, UK), synaptophysin (rabbit polyclonal, 1:500; Sigma-Aldrich, St Louis, MO, USA), GFAP (chicken polyclonal, 1:500; Millipore), and TNF-α (rabbit polyclonal, 1:100; Abcam). After washing, the sections were incubated with the corresponding secondary antibodies, Cy3-labeled anti-rabbit IgG (1:500; Jackson ImmunoResearch, West Grove, PA, USA) and FITC-labeled anti-chicken IgG (1:500; Millipore) for 2h at room temperature. DAPI (Dojindo, Kumamoto, Japan) was used for nuclear staining, and images were obtained using confocal laser scanning microscopy (Nikon A1, Tokyo, Japan).

For quantitative comparisons, the number of NeuN positive cells and the areas of GFAP-positivity were evaluated in a total of 6 different fields per animal (2 fields of 200 × 200μm per section). The intensities of 4HNE and synaptophysin staining were measured in a total of 15 different fields per animal (5 fields of 50 × 50μm per section), and the ratio of TNF-α positive area to GFAP positive area was analyzed within a total of 9 different fields per animal (3 fields of 50 × 50μm per section). All quantitative measurements were performed using Nikon NIS Elements AR software.

Isolation of BM-MSCs

Isolation of BM-MSCs was performed according to a previous study[23]. In brief, the bilateral femurs and tibias were removed and the bone marrows were flushed out using α-MEM medium (Gibco, Life Technology Japan, Tokyo, Japan) supplemented with 15% fetal bovine serum (CCB, Nichirei Bioscience, Tokyo, Japan) and 1% penicillin/streptomycin (Pen Strep, Life Technologies, Carlsbad, CA, USA), after removal of cancellous bone. The collected cells were incubated in 15cm dishes with 20ml α-MEM culture medium, and maintained at 37℃ in 5% CO_2. The culture medium was changed twice a week, and the cultivated BM-MSCs were used for further analysis. We previously confirmed that isolated BM-MSCs expressed the CD90 marker but not CD45 and CD11b, and were capable of differentiating into osteoblasts, adipocytes and chondrocyte-like cells[23].

BM-MSC phase contrast microscopy

The morphological images of BM-MSCs were obtained by phase contrast microscopy (Eclipse TE200; Nikon, Tokyo, Japan). To evaluate the length of the minor axis, Image J software[59] was used to measure the smallest length passing the nucleus orthogonal to the long axis. For quantitative analyses of the minor axis, all cells in 5 randomly selected fields at 20 × magnification was counted for each rat (n = 3/groups).

BM-MSC proliferation assays

The number of cells was indirectly analyzed using a Cell Counting Kit-8 (CCK-8; Dojindo Laboratories). Using 96-well culture plates (Corning Costar, Sigma-Aldrich), 3.0×10^3 of BM-MSCs were seeded in 3 wells for each sample. After 24h, 48h and 72h incubations, WST-8 solution was added and cells were cultured for a further 2h. The absorbance was measured with a microplate reader (Infinite M1000 Pro, TECAN, Mannedorf, Switzerland) at 490nm (n = 10-12/groups).

Scratch assay

Cell migration into the wound area was measured after scratching a confluent layer of BM-MSCs in a 35 mm dish. The BM-MSC monolayer was scratched with a pipette tip creating a wound in a cross shape and cells were cultured for a further 12h. After scratching, phase contrast time-lapse images were obtained by Axio Observer Z1 (Carl Zeiss, Oberkochen, Germany) using an enclosed incubation system (TOKAI HIT, Fujinomiya, Japan). The ratio of open area at 12h to open area at 0h was analyzed at 5 time points per sample using Image J software[59] (n = 3 /groups).

Intravenous injection of BM-MSCs

At 12 weeks after STZ ip injections of mice, STZ/CC MSCs or STZ/EE MSCs (1×10^4/g body weight) or Vehicle (200μl of PBS) were injected 4 times via the tail vein, at 2-week intervals. We selected the three BM-MSC samples closest to the median in each group according to the MTT assay, and mixed them evenly before intravenous injection.

Isolation of exosomes

Exosomes were isolated from conditioned BM-MSC media, rat sera and mouse sera using methodology described in a previous report[60]. Briefly, when BM-MSCs reached 60-80% confluency in 15cm dishes, the conventional medium was replaced with medium containing exosome-depleted fetal bovine serum (EXO-FBS-50 A-1 System Biosciences, Mountain View, CA, USA). After incubation for an additional 48h, the total culture medium (20ml) was collected, and the numbers of BM-MSCs were counted. The culture medium was centrifuged at 3,000g for 15 min, and the supernatant volume corresponding to 2.0×10^6 BM-MSCs was mixed with ExoQuick-TC (5:1) (System Biosciences). For example, for 4.0×10^6 BM-MSCs, 10ml (the volume corresponding to 2.0×10^6 cells) was mixed with 2ml of ExoQuick-TC. For the isolation of exosomes from rat and mouse sera, ExoQuick (System Biosciences) was used according to the manufacturer's protocol. Briefly, 250μl of rat serum and 150μl of mouse serum were mixed with 63μl and 37.8μl of ExoQuick solution, respectively. After incubating overnight at 4℃, the mixture was centrifuged at 1,500g for 30min. The resulting exosome pellets were immediately used for RNA isolation or western blotting.

miRNA isolation and quantitation

Total miRNAs were extracted from isolated exosomes using a mirVana™ PARIS™ Kit (Thermo Fisher Scientific, Waltham, MA, USA), and 2μL of 2nM exogenous synthetic cel-miR-39

was used as an external control to normalize each miRNA evaluation. Following RNA isolation, a TaqMan Advanced miRNA cDNA Synthesis kit (Thermo Fisher Scientific) was used for reverse transcription, and real time PCR was carried out using the TaqMan Fast Advanced Master Mix (Thermo Fisher Scientific). The relative quantities of miR-146a and miR-181a were assessed by the comparative Ct method ($2^{-\Delta\Delta Ct}$).

Statistical Analysis

Data were expressed as means ± standard error (SE). Statistical analysis was performed using R software (version3.3.2) by one-way analysis of variance (ANOVA), followed by Bonferroni post hoc analysis. When interactions between two factors were considered, two-way ANOVA with a Bonferroni post hoc was performed for analysis. The difference was designated as statistically significant when $P = 0.05$ or less.

References

1 Ott, A. *et al.* Diabetes mellitus and the risk of dementia: The Rotterdam Study. *Neurology* **53**, 1937-1942 (1999).

2 Biessels, G. J., Staekenborg, S., Brunner, E., Brayne, C. & Scheltens, P. Risk of dementia in diabetes mellitus: a systematic review. *Lancet Neurol* **5**, 64-74 (2006).

3 Son, H. *et al.* Type 1 diabetes alters astrocytic properties related with neurotransmitter supply, causing abnormal neuronal activities. *Brain research* **1602**, 32-43 (2015).

4 Revsin, Y. *et al.* Neuronal and astroglial alterations in the hippocampus of a mouse model for type 1 diabetes. *Brain research* **1038**, 22-31 (2005).

5 Min, L. J. *et al.* Peroxisome proliferator-activated receptor-gamma activation with angiotensin II type 1 receptor blockade is pivotal for the prevention of blood-brain barrier impairment and cognitive decline in type 2 diabetic mice. *Hypertension* **59**, 1079-1088 (2012).

6 Agrawal, R. *et al.* Deterioration of plasticity and metabolic homeostasis in the brain of the UCD-T2DM rat model of naturally occurring type-2 diabetes. *Biochim Biophys Acta* **1842**, 1313-1323 (2014).

7 Practice guideline for the treatment of patients with Alzheimer's disease and other dementias of late life. American Psychiatric Association. *Am J Psychiatry* **154**, 1-39 (1997).

8 Clare, L., Woods, R. T., Moniz Cook, E. D., Orrell, M. & Spector, A. Cognitive rehabilitation

and cognitive training for early-stage Alzheimer's disease and vascular dementia. *Cochrane Database Syst Rev*, CD003260 (2003).

9 van Praag, H., Kempermann, G. & Gage, F. H. Neural consequences of environmental enrichment. *Nature reviews. Neuroscience* **1**, 191-198 (2000).

10 Li, S. *et al.* Environmental novelty activates beta2-adrenergic signaling to prevent the impairment of hippocampal LTP by Abeta oligomers. *Neuron* **77**, 929-941 (2013).

11 Klaissle, P. *et al.* Physical activity and environmental enrichment regulate the generation of neural precursors in the adult mouse substantia nigra in a dopamine-dependent manner. *BMC neuroscience* **13**, 132 (2012).

12 Nithianantharajah, J. & Hannan, A. J. Enriched environments, experience-dependent plasticity and disorders of the nervous system. *Nature reviews. Neuroscience* **7**, 697-709 (2006).

13 Beauquis, J., Roig, P., De Nicola, A. F. & Saravia, F. Short-term environmental enrichment enhances adult neurogenesis, vascular network and dendritic complexity in the hippocampus of type 1 diabetic mice. *PloS one* **5**, e13993 (2010).

14 Cao, W. *et al.* Early enriched environment induces an increased conversion of proBDNF to BDNF in the adult rat's hippocampus. *Behavioural brain research* **265**, 76-83 (2014).

15 Del Arco, A., Segovia, G., Garrido, P., de Blas, M. & Mora, F. Stress, prefrontal cortex and environmental enrichment: studies on dopamine and acetylcholine release and working

memory performance in rats. *Behavioural brain research* **176**, 267-273 (2007).

16 During, M. J. & Cao, L. VEGF, a mediator of the effect of experience on hippocampal neurogenesis. *Curr Alzheimer Res* **3**, 29-33 (2006).

17 Jung, C. K. & Herms, J. Structural dynamics of dendritic spines are influenced by an environmental enrichment: an in vivo imaging study. *Cerebral cortex* **24**, 377-384 (2014).

18 Fischer, A., Sananbenesi, F., Wang, X., Dobbin, M. & Tsai, L. H. Recovery of learning and memory is associated with chromatin remodelling. *Nature* **447**, 178-182 (2007).

19 Pusic, K. M., Pusic, A. D. & Kraig, R. P. Environmental Enrichment Stimulates Immune Cell Secretion of Exosomes that Promote CNS Myelination and May Regulate Inflammation. *Cell Mol Neurobiol* **36**, 313-325 (2016).

20 Piazza, F. V. *et al.* Enriched environment induces beneficial effects on memory deficits and microglial activation in the hippocampus of type 1 diabetic rats. *Metab Brain Dis* **29**, 93-104 (2014).

21 Piazza, F. V. *et al.* Enriched environment prevents memory deficits in type 1 diabetic rats. *Behavioural brain research* **217**, 16-20 (2011).

22 Nakano, M. *et al.* Bone marrow-derived mesenchymal stem cells improve diabetes-induced cognitive impairment by exosome transfer into damaged neurons and astrocytes. *Sci Rep* **6**, 24805 (2016).

23 Nagaishi, K., Ataka, K., Echizen, E., Arimura, Y. & Fujimiya, M. Mesenchymal stem cell

therapy ameliorates diabetic hepatocyte damage in mice by inhibiting infiltration of bone marrow-derived cells. *Hepatology* **59**, 1816-1829 (2014).

24 Nagaishi, K. *et al.* Mesenchymal stem cell therapy ameliorates diabetic nephropathy via the paracrine effect of renal trophic factors including exosomes. *Sci Rep* **6**, 34842 (2016).

25 Xu, J. *et al.* The role of microRNA-146a in the pathogenesis of the diabetic wound-healing impairment: correction with mesenchymal stem cell treatment. *Diabetes* **61**, 2906-2912 (2012).

26 Ma, S. *et al.* Immunobiology of mesenchymal stem cells. *Cell Death Differ* **21**, 216-225 (2014).

27 Yan, J. *et al.* Type 2 diabetes restricts multipotency of mesenchymal stem cells and impairs their capacity to augment postischemic neovascularization in db/db mice. *J Am Heart Assoc* **1**, e002238 (2012).

28 Thery, C. Exosomes: secreted vesicles and intercellular communications. *F1000 Biol Rep* **3**, 15 (2011).

29 Bian, S. *et al.* Extracellular vesicles derived from human bone marrow mesenchymal stem cells promote angiogenesis in a rat myocardial infarction model. *J Mol Med* **92**, 387-397 (2014).

30 Bruno, S., Porta, S. & Bussolati, B. Extracellular vesicles in renal tissue damage and regeneration. *Eur J Pharmacol* **790**, 83-91 (2016).

31 Xin, H. *et al.* MiR-133b promotes neural plasticity and functional recovery after treatment of stroke with multipotent mesenchymal stromal cells in rats via transfer of exosome-enriched extracellular particles. *Stem cells* **31**, 2737-2746 (2013).

32 Li, Y., Liu, Z., Xin, H. & Chopp, M. The role of astrocytes in mediating exogenous cell-based restorative therapy for stroke. *Glia* **62**, 1-16 (2014).

33 Elbana, A. M., Abdel-Salam, S., Morad, G. M. & Omran, A. A. Role of Endogenous Bone Marrow Stem Cells Mobilization in Repair of Damaged Inner Ear in Rats. *Int J Stem Cells* **8**, 146-154 (2015).

34 Chang, T. C., Hsu, M. F. & Wu, K. K. High glucose induces bone marrow-derived mesenchymal stem cell senescence by upregulating autophagy. *PloS one* **10**, e0126537 (2015).

35 Sethe, S., Scutt, A. & Stolzing, A. Aging of mesenchymal stem cells. *Ageing Res Rev* **5**, 91-116 (2006).

36 Turinetto, V., Vitale, E. & Giachino, C. Senescence in Human Mesenchymal Stem Cells: Functional Changes and Implications in Stem Cell-Based Therapy. *Int J Mol Sci* **17**, 7 (2016).

37 Wyles, C. C. *et al.* Differential cytotoxicity of corticosteroids on human mesenchymal stem cells. *Clin Orthop Relat Res* **473**, 1155-1164 (2015).

38 Nagayach, A., Patro, N. & Patro, I. Astrocytic and microglial response in experimentally induced diabetic rat brain. *Metab Brain Dis* **29**, 747-761 (2014).

39 Coleman, E., Judd, R., Hoe, L., Dennis, J. & Posner, P. Effects of diabetes mellitus on astrocyte GFAP and glutamate transporters in the CNS. *Glia* **48**, 166-178 (2004).

40 Gong, P. *et al.* Phosphorylation of mitogen- and stress-activated protein kinase-1 in astrocytic inflammation: a possible role in inhibiting production of inflammatory cytokines. *PloS one* **8**, e81747 (2013).

41 Sofroniew, M. V. & Vinters, H. V. Astrocytes: biology and pathology. *Acta Neuropathol* **119**, 7-35 (2010).

42 Diniz, L. P. *et al.* Astrocyte-induced synaptogenesis is mediated by transforming growth factor beta signaling through modulation of D-serine levels in cerebral cortex neurons. *J Biol Chem* **287**, 41432-41445 (2012).

43 Watts, L. T., Rathinam, M. L., Schenker, S. & Henderson, G. I. Astrocytes protect neurons from ethanol-induced oxidative stress and apoptotic death. *Journal of neuroscience research* **80**, 655-666 (2005).

44 Ouyang, Y. B., Xu, L., Liu, S. & Giffard, R. G. Role of Astrocytes in Delayed Neuronal Death: GLT-1 and its Novel Regulation by MicroRNAs. *Adv Neurobiol* **11**, 171-188 (2014).

45 Olmos, G. & Llado, J. Tumor necrosis factor alpha: a link between neuroinflammation and excitotoxicity. *Mediators Inflamm* **2014**, 861231 (2014).

46 Morrison, J. H. & Baxter, M. G. The ageing cortical synapse: hallmarks and implications for cognitive decline. *Nature reviews. Neuroscience* **13**, 240-250 (2012).

47 Saba, R., Sorensen, D. L. & Booth, S. A. MicroRNA-146a: A Dominant, Negative Regulator of the Innate Immune Response. *Front Immunol* **5**, 578 (2014).

48 Iyer, A. *et al.* MicroRNA-146a: a key regulator of astrocyte-mediated inflammatory response. *PloS one* **7**, e44789 (2012).

49 Baldeon, R. L. *et al.* Decreased serum level of miR-146a as sign of chronic inflammation in type 2 diabetic patients. *PloS one* **9**, e115209 (2014).

50 Bhatt, K. *et al.* Anti-Inflammatory Role of MicroRNA-146a in the Pathogenesis of Diabetic Nephropathy. *JASN* **27**, 2277-2288 (2016).

51 Wang, L. *et al.* The role of miR-146a in dorsal root ganglia neurons of experimental diabetic peripheral neuropathy. *Neuroscience* **259**, 155-163 (2014).

52 Ti, D., Hao, H., Fu, X. & Han, W. Mesenchymal stem cells-derived exosomal microRNAs contribute to wound inflammation. *Sci China Life Sci* **59**, 1305-1312 (2016).

53 Nahid, M. A., Pauley, K. M., Satoh, M. & Chan, E. K. miR-146a is critical for endotoxin-induced tolerance: IMPLICATION IN INNATE IMMUNITY. *J Biol Chem* **284**, 34590-34599 (2009).

54 Hutchison, E. R. *et al.* Evidence for miR-181 involvement in neuroinflammatory responses of astrocytes. *Glia* **61**, 1018-1028 (2013).

55 Gutierrez-Fernandez, M. *et al.* Trophic factors and cell therapy to stimulate brain repair after ischaemic stroke. *J Cell Mol Med* **16**, 2280-2290 (2012).

56 Fares, R. P. *et al.* Standardized environmental enrichment supports enhanced brain plasticity in healthy rats and prevents cognitive impairment in epileptic rats. *PloS one* **8**, e53888 (2013).

57 Ohta, H., Nishikawa, H., Kimura, H., Anayama, H. & Miyamoto, M. Chronic cerebral hypoperfusion by permanent internal carotid ligation produces learning impairment without brain damage in rats. *Neuroscience* **79**, 1039-1050 (1997).

58 Zhou, G., Xiong, W., Zhang, X. & Ge, S. Retrieval of Consolidated Spatial Memory in the Water Maze Is Correlated with Expression of pCREB and Egr1 in the Hippocampus of Aged Mice. *Dementia and geriatric cognitive disorders extra* **3**, 39-47 (2013).

59 Schneider, C. A., Rasband, W. S. & Eliceiri, K. W. NIH Image to ImageJ: 25 years of image analysis. *Nat Methods* **9**, 671-675 (2012).

60 Kang, K. *et al.* Exosomes Secreted from CXCR4 Overexpressing Mesenchymal Stem Cells Promote Cardioprotection via Akt Signaling Pathway following Myocardial Infarction. *Stem cells international* **2015**, 659890 (2015).

Acknowledgements

The author would like to thank Yuko Hayakawa, Kozue Kamiya, Tatsuya Shiraishi for technical support and Yoshiyuki Kanazawa for manufacture of EE cage.

Author Contributions

K.K. designed the study, performed the experiments, analyzed the data, and wrote the paper. M.F. and M.N. coordinated the study and wrote the paper. E.K., Y.M., T.C., M.O., and K.N. supported analysis of the data and reviewed the paper.

FIGURE LEGENDS

Figure 1. Effects of an EE on cognitive function in STZ-diabetic rats

(a) EE equipment and experimental protocols. After STZ or vehicle injection, Control/CC and STZ/CC rats are housed in conventional cages (CC), and STZ/EE rats are housed in enriched environment (EE) cages. After 8 weeks in CC or EE cages, the Morris water maze (MWM) tests are carried out. (b) Changes in body weight and serum blood glucose level from 1 to 8 weeks after STZ injection. $^{*}P < 0.01$, Control vs STZ/CC and STZ/EE, two-way ANOVA, Bonferroni post hoc test. Values are means ± SE, n = 10-12. (c) MWM test. In the hidden training test, STZ/CC rats have a longer escape latency than Control/CC rats on days 2, 3 and 4. On the other hand, STZ/EE rats have a shortened latency compared to the STZ/CC rats on days 3 and 4. $^{*}P < 0.01$, Day 2; Control/CC vs STZ/CC, Day 3, 4; Control/CC and STZ/EE vs STZ/CC, two-way ANOVA ($F(2,129) = 47.1$ $P < 0.01$), Bonferroni post hoc test. Values are means ± SE, n = 10-12. During the probe test, the time that Control/CC rats and STZ/EE rats spent in the SE target quadrant is significantly longer than in other areas. In contrast, the time STZ/CC rats spent in the SE target quadrant is not significantly different from time spent in other quadrants. (Control/CC; $^{*}P < 0.01$, SE vs NE, SW and NW, STZ/EE; $^{\dagger}P < 0.05$, SE vs NE and NW, $^{\dagger\dagger}P < 0.01$, SE vs SW, one-way ANOVA, Bonferroni post hoc test).

Figure 2. Morphological analysis of the rat hippocampal CA1 region

(a) The number of NeuN-positive cells in the hippocampal CA1 region of STZ/CC rats is significantly lower than Control/CC rats, while that of STZ/EE rats is significantly higher than STZ/CC rats. (b) The intensity of the 4HNE (4-hydroxynonenal)-positive area is significantly increased in STZ/CC rats, and this increase is not evident in STZ/EE rats which are similar to controls. (c) The intensity of synaptophysin staining is significantly decreased in STZ/CC rats, while STZ/EE have a significantly higher intensity than STZ/CC and Control/CC rats. (d) There is no differences in the area of GFAP-positivity reaction among the three groups. (e) The ratio of TNF-α positive area to GFAP positive area is significantly increased in STZ/CC rats; however, the ratio in STZ/EE rats is similar to controls. (a-e) $^{*}P < 0.05$, $^{**}P < 0.01$, one-way ANOVA, Bonferroni post hoc test. Values are means ± SE, n = 3-4.

Figure 3. Comparison of BM-MSCs isolated from Control/CC, STZ/CC and STZ/EE rats

(a) Phase-contrast microscopy analysis. Control/CC BM-MSCs are slim and spindle shaped with long cytoplasmic processes similar to STZ/EE BM-MSCs. STZ/CC BM-MSCs are flat and broad. The minor axis of the cells is significantly longer in STZ/CC rats, while the length in STZ/EE rats is similar to normal. $^{*}P < 0.05$, one-way ANOVA, Bonferroni post hoc test. Values are means ± SE, n = 3. (b) In the MTT assays the proliferation of STZ/CC BM-MSCs is reduced compared to Control/CC BM-MSCs at 48h and 72h. However, STZ/EE BM-MSC proliferation is significantly greater than STZ/CC BM-MSCs at 72h. $^{*}P < 0.05$, $^{**}P < 0.01$, 48 h; Control/CC vs STZ/CC, 72 h;

Control/CC and STZ/EE vs STZ/CC, two-way ANOVA, Bonferroni post hoc test. Values are means ± SE, n = 10-12. (c) In the scratch assays the open wound area is significantly larger in STZ/CC BM-MSC cultures compared with Control/CC cultures, while the area in STZ/EE BM-MSC cultures is smaller than STZ/CC cultures at 12h. $^{*}P < 0.05$, $^{**}P < 0.01$, one-way ANOVA, Bonferroni post hoc test. Values are means ± SE, n = 3.

Figure 4. Intravenous injection of BM-MSCs isolated from STZ/CC or STZ/EE rats into STZ-induced diabetic mice

(a) Experimental protocol. Vehicle, STZ/CC or STZ/EE BM-MSCs (1×10^4/g body weight) are administered intravenously from 12 weeks after STZ injections, 4 times at 2-weeks intervals. Two weeks after the last injection, the MWM test is performed. (b) No significant changes are detected in body weight and blood glucose levels among the three groups at the 20th week after STZ injection. One-way ANOVA. Values are means ± SE, n = 10. (c) MWM test. In the hidden platform test STZ/EE BM-MSC iv mice have a shorter escape latency than Vehicle iv mice and STZ/CC BM-MSC iv mice on day 4. $^{*}P < 0.01$, STZ/EE BM-MSC iv vs Vehicle iv and STZ/CC BM-MSC iv, two-way ANOVA ($F(2,117) = 5.62$, $P < 0.01$), Bonferroni post hoc test. Values are means ± SE, n = 10. During the probe test the time spent in the SE quadrant compared with other quadrants is not significantly different between the Vehicle iv and STZ/CC BM-MSC iv groups. In contrast, the time spent in the SE quadrant is significantly longer than in other quadrants in the STZ/EE BM-MSC iv

group. $^{*}P < 0.01$, SE vs NE, SW and NW, one-way ANOVA, Bonferroni post hoc test.

Figure 5. Morphological analysis of the CA1 region in mice

(a) There are no significant differences in the number of NeuN-positive cells between the three groups. (b) The intensity of 4HNE staining in the CA1 region from STZ/EE BM-MSC iv mice is significantly decreased compared to Vehicle iv or STZ/CC BM-MSC iv mice. (c) The intensity of synaptophysin staining in the CA1 region of STZ/EE BM-MSC iv mice is significantly increased compared with Vehicle iv or STZ/CC BM-MSC iv mice. (d) There are no significant differences in the GFAP positive area in the CA1 region among the three groups. (e) The ratio of TNF-α positive area to GFAP positive area in STZ/EE BM-MSC iv mice is significantly decreased compared with Vehicle iv or STZ/CC BM-MSC iv mice. $^{*}P < 0.05$, $^{**}P < 0.01$, one-way ANOVA, Bonferroni post hoc test. Values are means ± SE, n = 3-4.

Figure 6. Analysis of exosomal miRNA in BM-MSC conditioned medium and mouse and rat sera

(a) The CD63 and HSP70 exosomal markers are detected by western blotting of exosomes extracted from conditioned medium from cultured BM-MSCs, or from mouse and rat sera. (b) The concentration of miR-146a in exosomes released by STZ/CC BM-MSCs is significantly lower than Control/CC BM-MSCs, while the levels in STZ/EE BM-MSCs are significantly higher than those in

STZ/CC BM-MSCs, n = 4-5. (c) The serum levels of exosomal miR-146a in STZ/EE BM-MSC iv mice are significantly higher than those in Vehicle iv and STZ/CC BM-MSC iv mice, n = 7-10. (d) The serum levels of exosomal miR-146a in STZ/CC rats are significantly lower than Control/CC, while the serum levels of exosomal miR-146a in STZ/EE rats are significantly higher than those in STZ/CC rats, n = 6-8. (e) There are no significant differences in exosomal miR-181a levels in BM-MSCs from the three groups, n = 5. (f) The serum levels of exosomal miR-181a in STZ/CC and STZ/EE rats are significantly decreased compared with those in Control/CC rats, n = 4-5. $^{*}P < 0.05$, $^{**}P < 0.01$, one-way ANOVA, Bonferroni post hoc test. Values are means ± SE.

Figure1

a

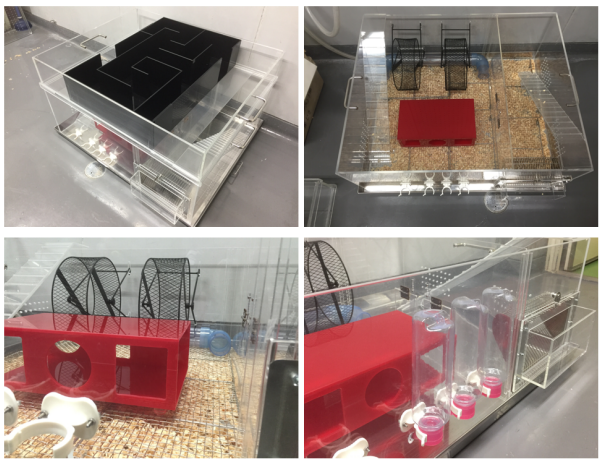

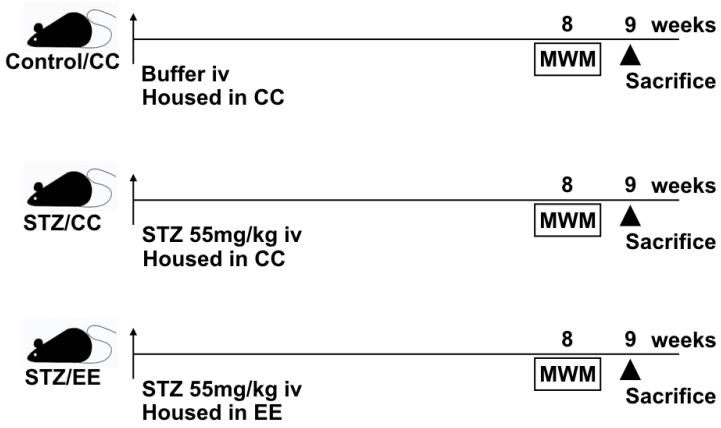
Control/CC
Buffer iv
Housed in CC
8
9 weeks
MWM
Sacrifice
STZ/CC
STZ 55mg/kg iv
Housed in CC
8
9 weeks
MWM
Sacrifice
STZ/EE
STZ 55mg/kg iv
Housed in EE
8
9 weeks
MWM
Sacrifice

b

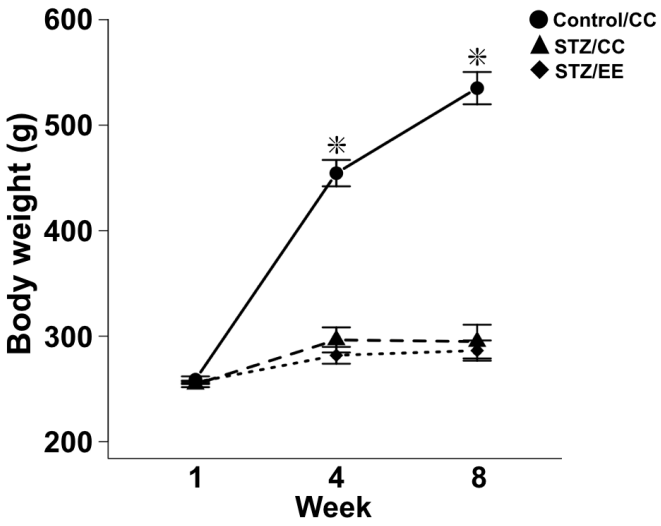
Body weight (g)
600
500
400
300
200
1
4
8
Week
Control/CC
STZ/CC
STZ/EE

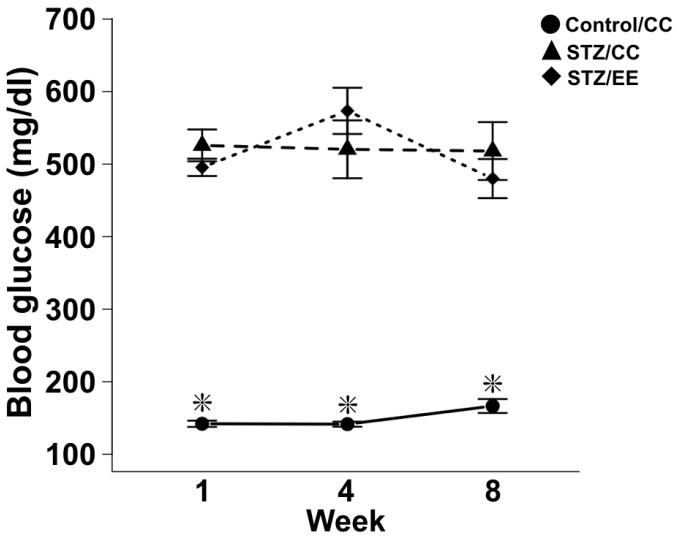
Blood glucose (mg/dl)
700
600
500
400
300
200
100
1
4
8
Week
Control/CC
STZ/CC
STZ/EE

c

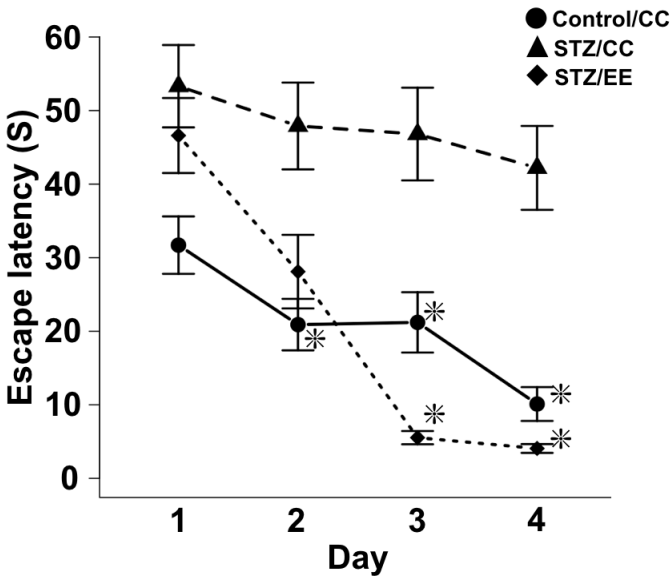
Escape latency (S)
60
50
40
30
20
10
0
1
2
3
4
Day
Control/CC
STZ/CC
STZ/EE

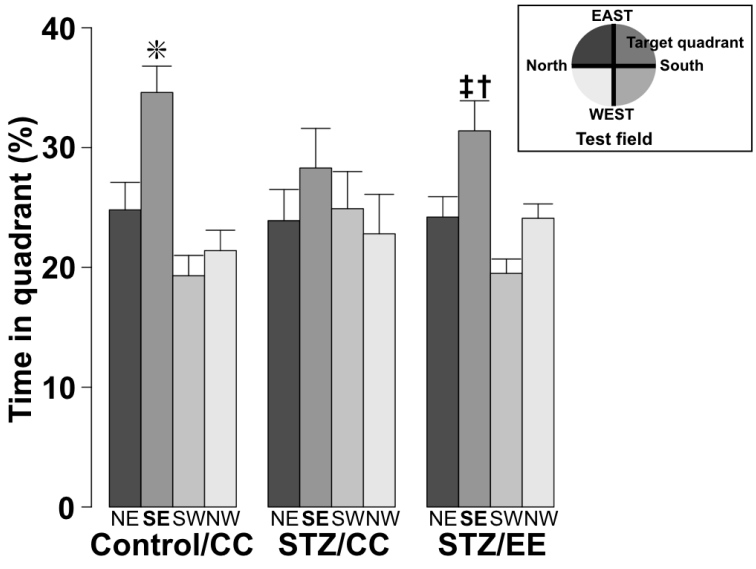
Time in quadrant (%)
40
30
20
10
0
NE SE SW NW
Control/CC
STZ/CC
STZ/EE
EAST
Target quadrant
North
South
WEST
Test field

Figure2

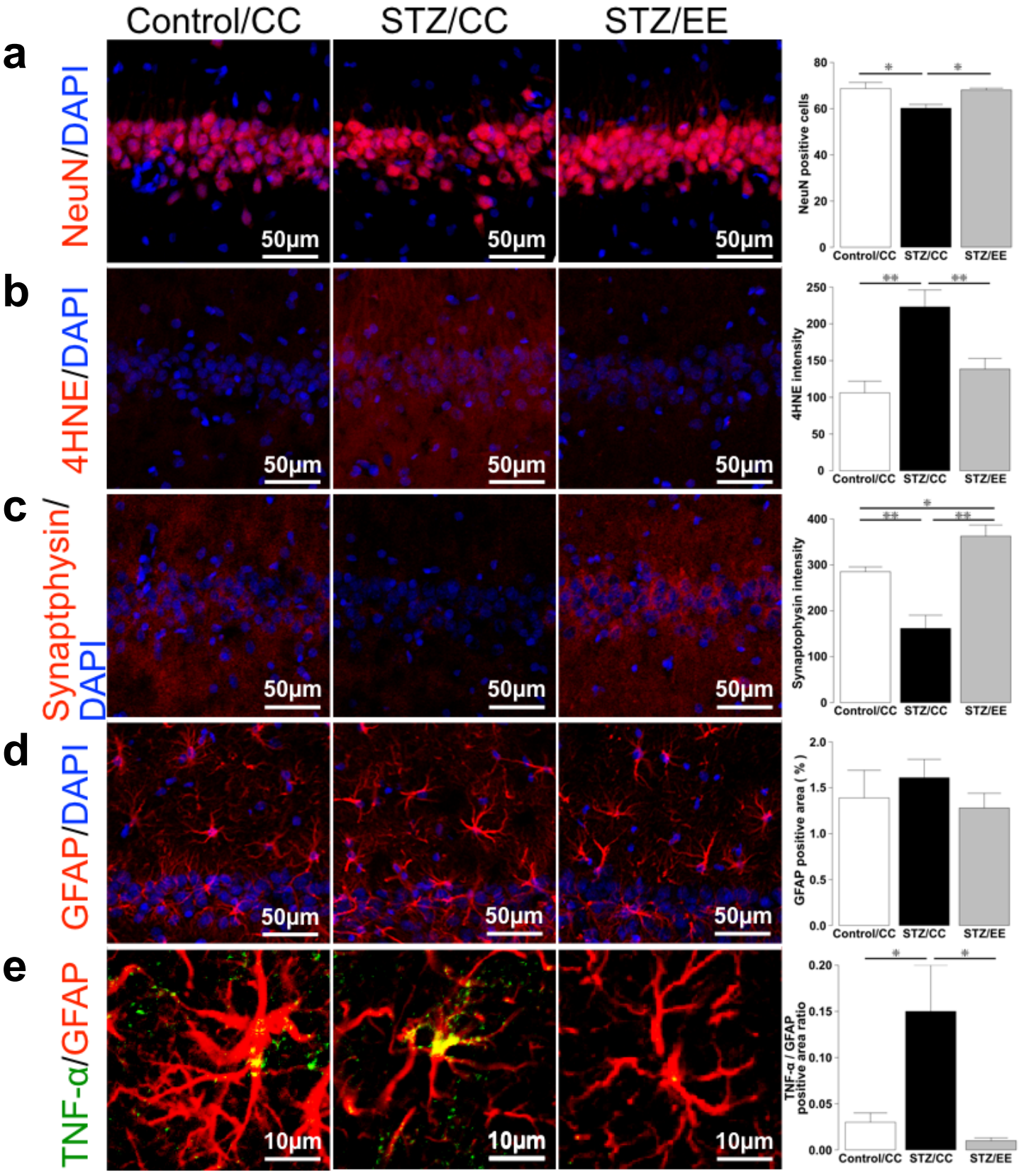
Control/CC
STZ/CC
STZ/EE
a
NeuN/DAPI
50μm
NeuN positive cells
b
4HNE/DAPI
4HNE intensity
c
Synaptophysin/
DAPI
Synaptophysin intensity
d
GFAP/DAPI
GFAP positive area (%)
e
TNF-α/GFAP
10μm
TNF-α / GFAP
positive area ratio

Figure3

a

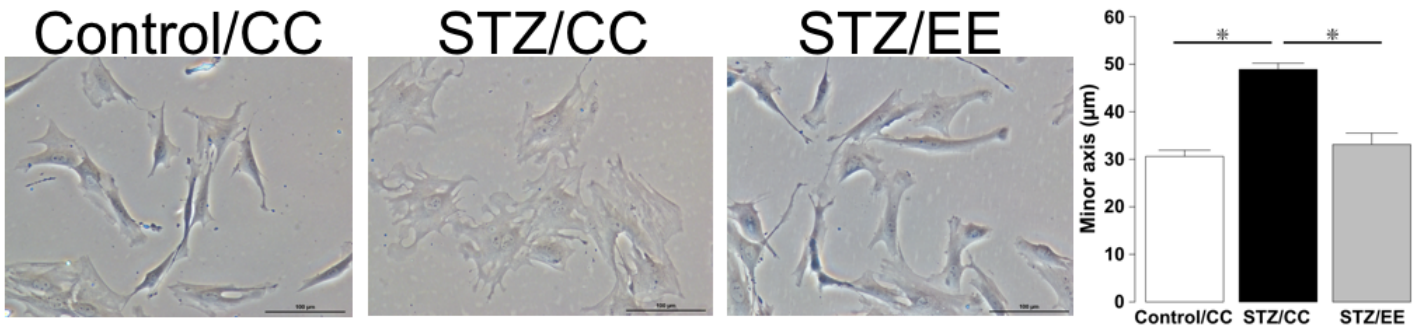
Control/CC
STZ/CC
STZ/EE
Minor axis (μm)
60
50
40
30
20
10
0
*
*
Control/CC
STZ/CC
STZ/EE

b

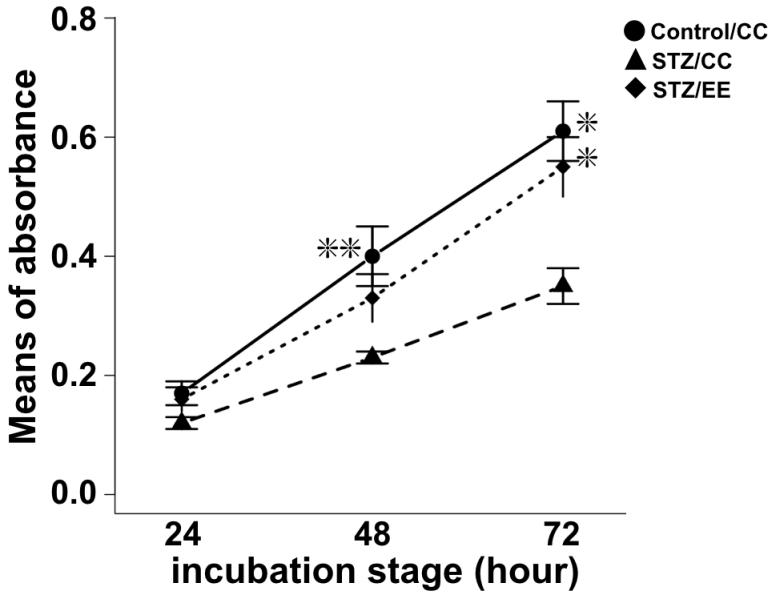
Means of absorbance
0.8
0.6
0.4
0.2
0.0
24
48
72
incubation stage (hour)
Control/CC
STZ/CC
STZ/EE
**
*
*

c

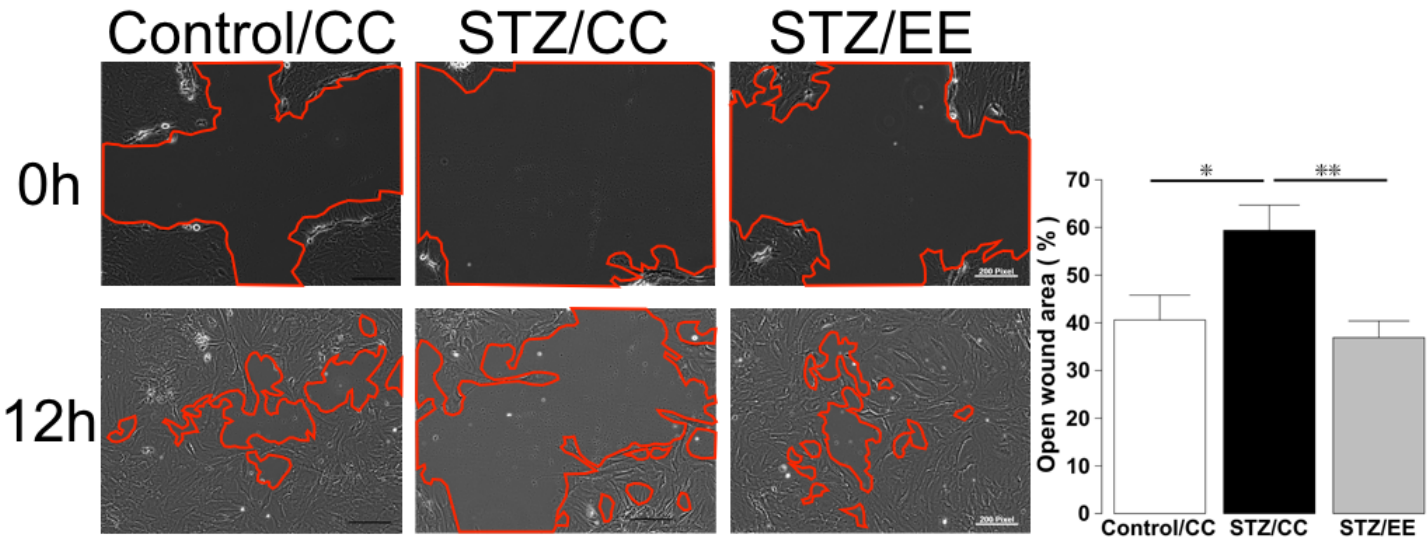
Control/CC
STZ/CC
STZ/EE
0h
12h
Open wound area (%)
70
60
50
40
30
20
10
0
*
**
Control/CC
STZ/CC
STZ/EE

Figure4

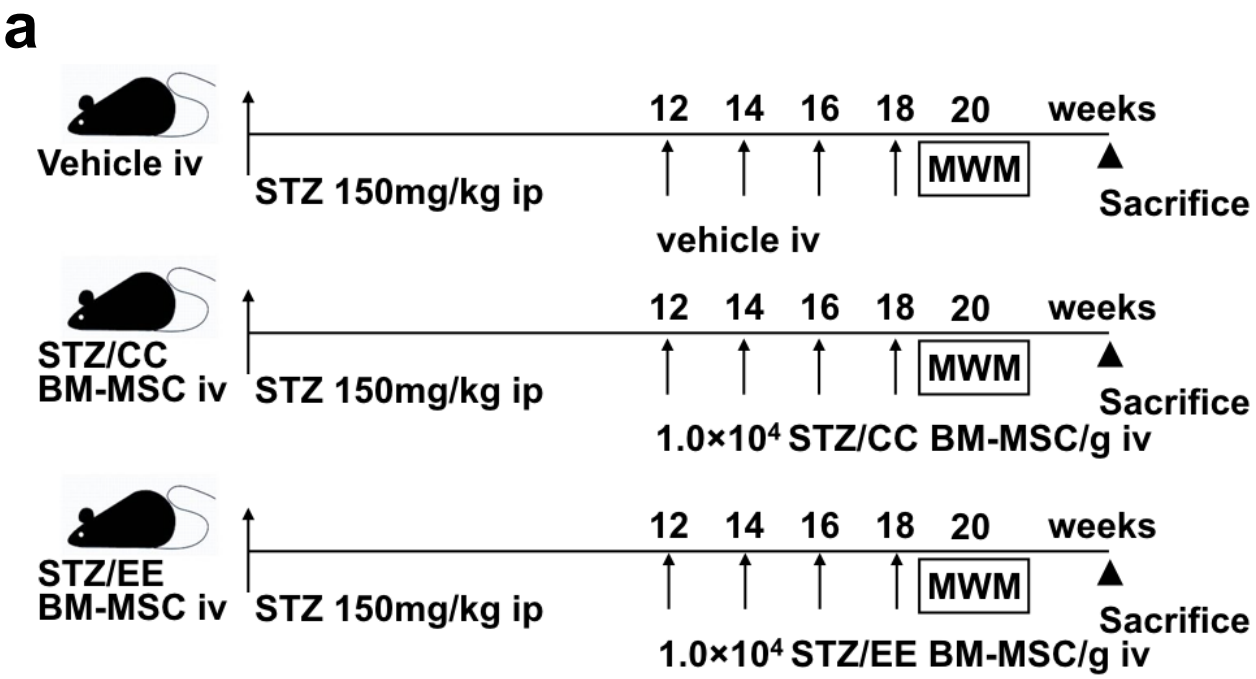
a
Vehicle iv
STZ 150mg/kg ip
12 14 16 18 20 weeks
MWM
Sacrifice
vehicle iv
STZ/CC
BM-MSC iv
STZ 150mg/kg ip
12 14 16 18 20 weeks
MWM
Sacrifice
1.0×10⁴ STZ/CC BM-MSC/g iv
STZ/EE
BM-MSC iv
STZ 150mg/kg ip
12 14 16 18 20 weeks
MWM
Sacrifice
1.0×10⁴ STZ/EE BM-MSC/g iv

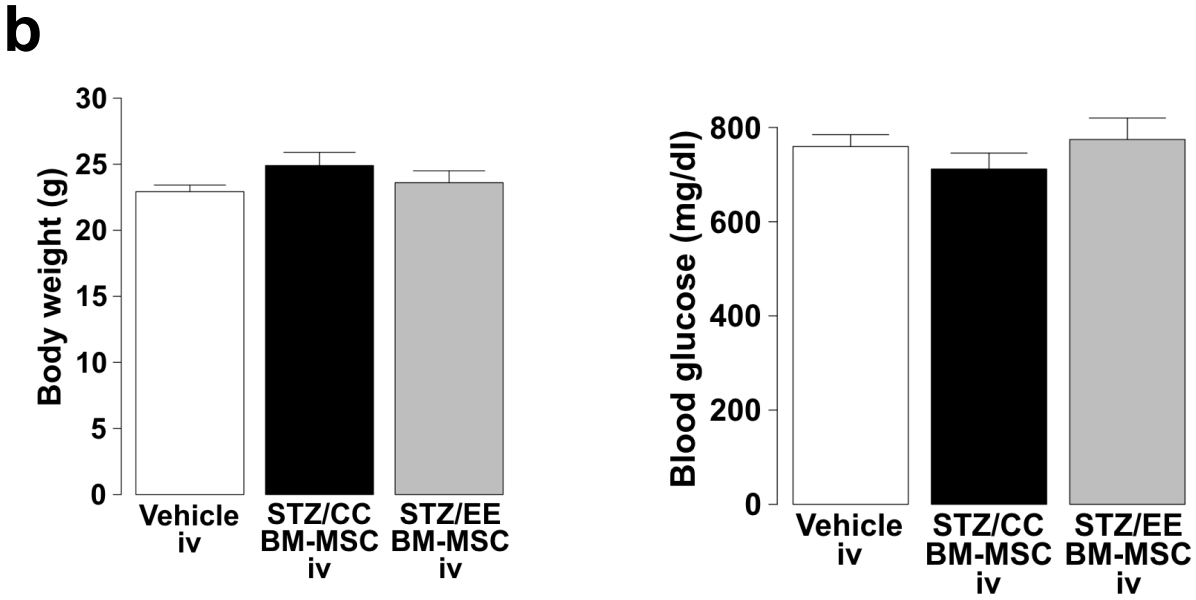
b
Body weight (g)
30
25
20
15
10
5
0
Vehicle iv
STZ/CC BM-MSC iv
STZ/EE BM-MSC iv
Blood glucose (mg/dl)
800
600
400
200
0
Vehicle iv
STZ/CC BM-MSC iv
STZ/EE BM-MSC iv

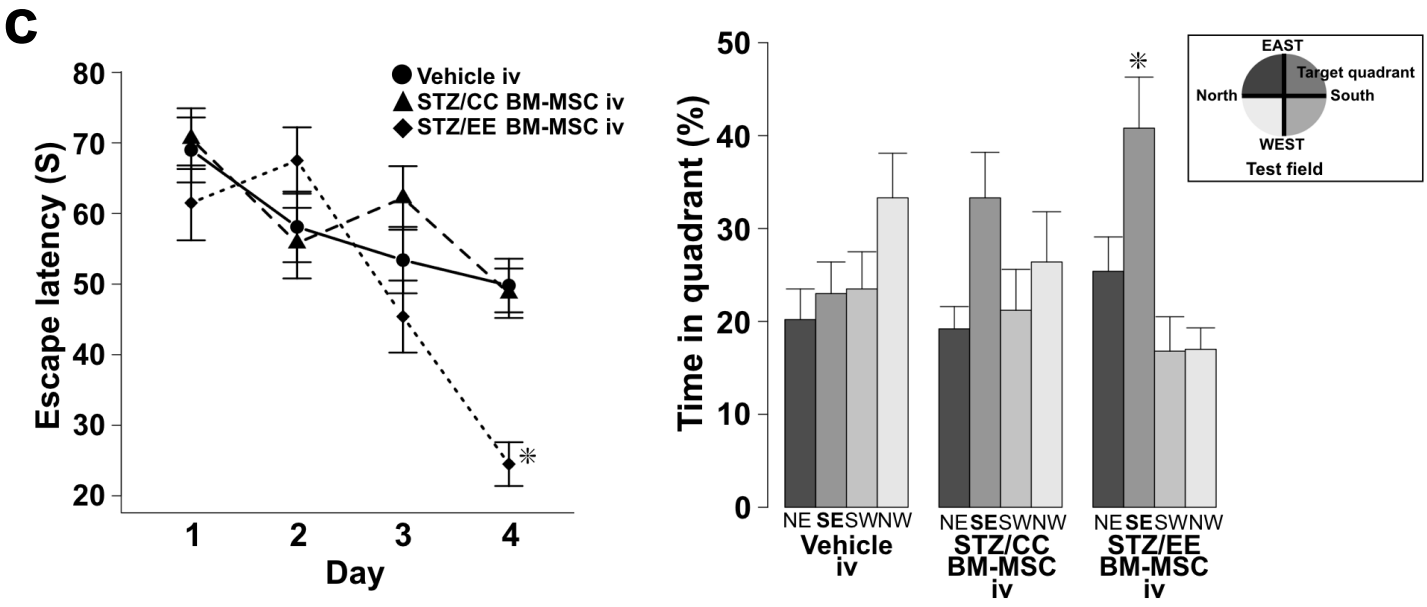
c
Escape latency (S)
80
70
60
50
40
30
20
1
2
3
4
Day
Vehicle iv
STZ/CC BM-MSC iv
STZ/EE BM-MSC iv
*
Time in quadrant (%)
50
40
30
20
10
0
NE SE SW NW
Vehicle iv
STZ/CC BM-MSC iv
STZ/EE BM-MSC iv
*
EAST
North
South
WEST
Target quadrant
Test field

Figure5

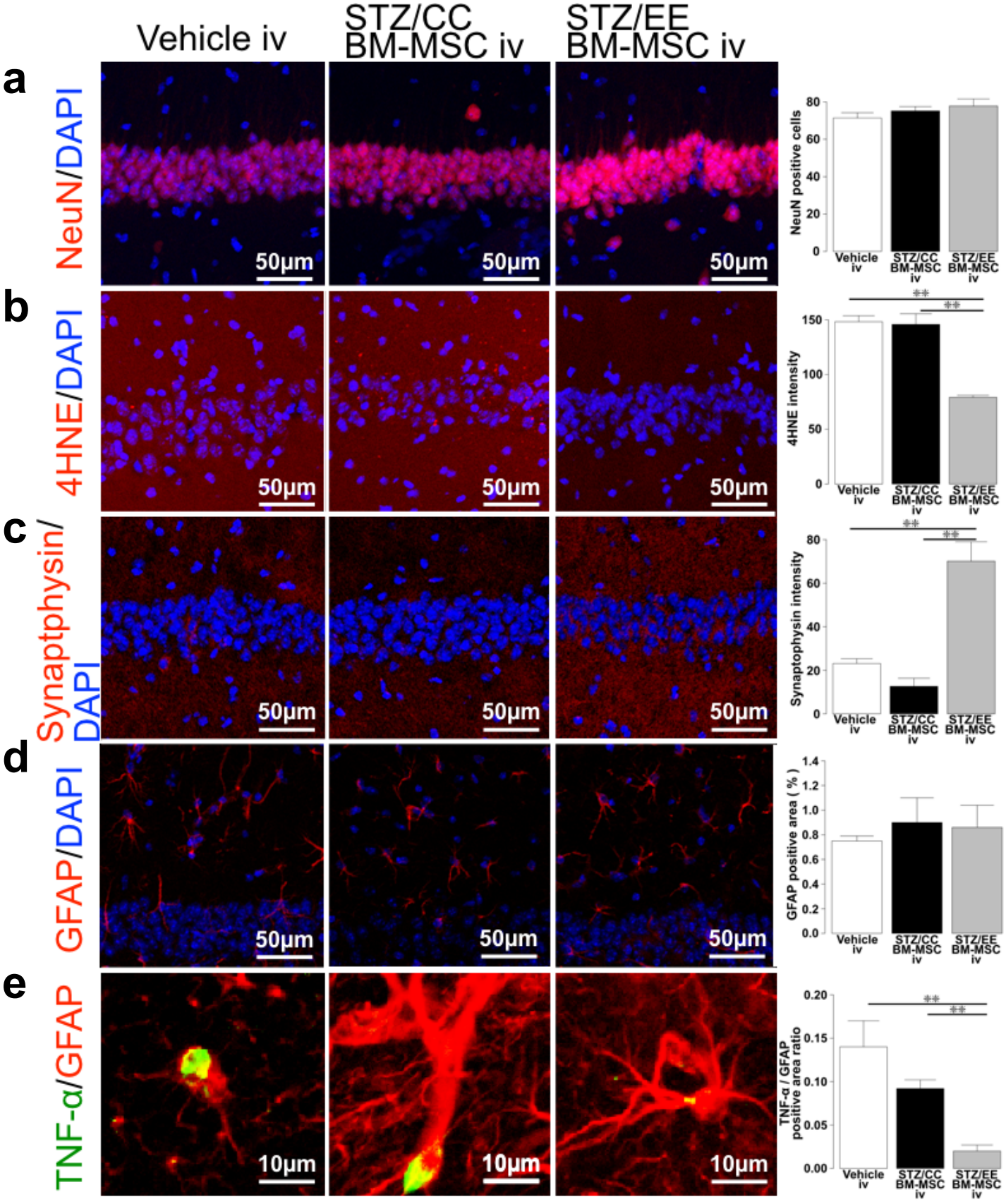
Vehicle iv
STZ/CC BM-MSC iv
STZ/EE BM-MSC iv
a
NeuN/DAPI
50μm
NeuN positive cells
Vehicle iv
STZ/CC BM-MSC iv
STZ/EE BM-MSC iv
b
4HNE/DAPI
4HNE intensity
**
c
Synaptophysin/ DAPI
Synaptophysin intensity
d
GFAP/DAPI
GFAP positive area (%)
e
TNF-α/GFAP
10μm
TNF-α / GFAP positive area ratio

Figure6

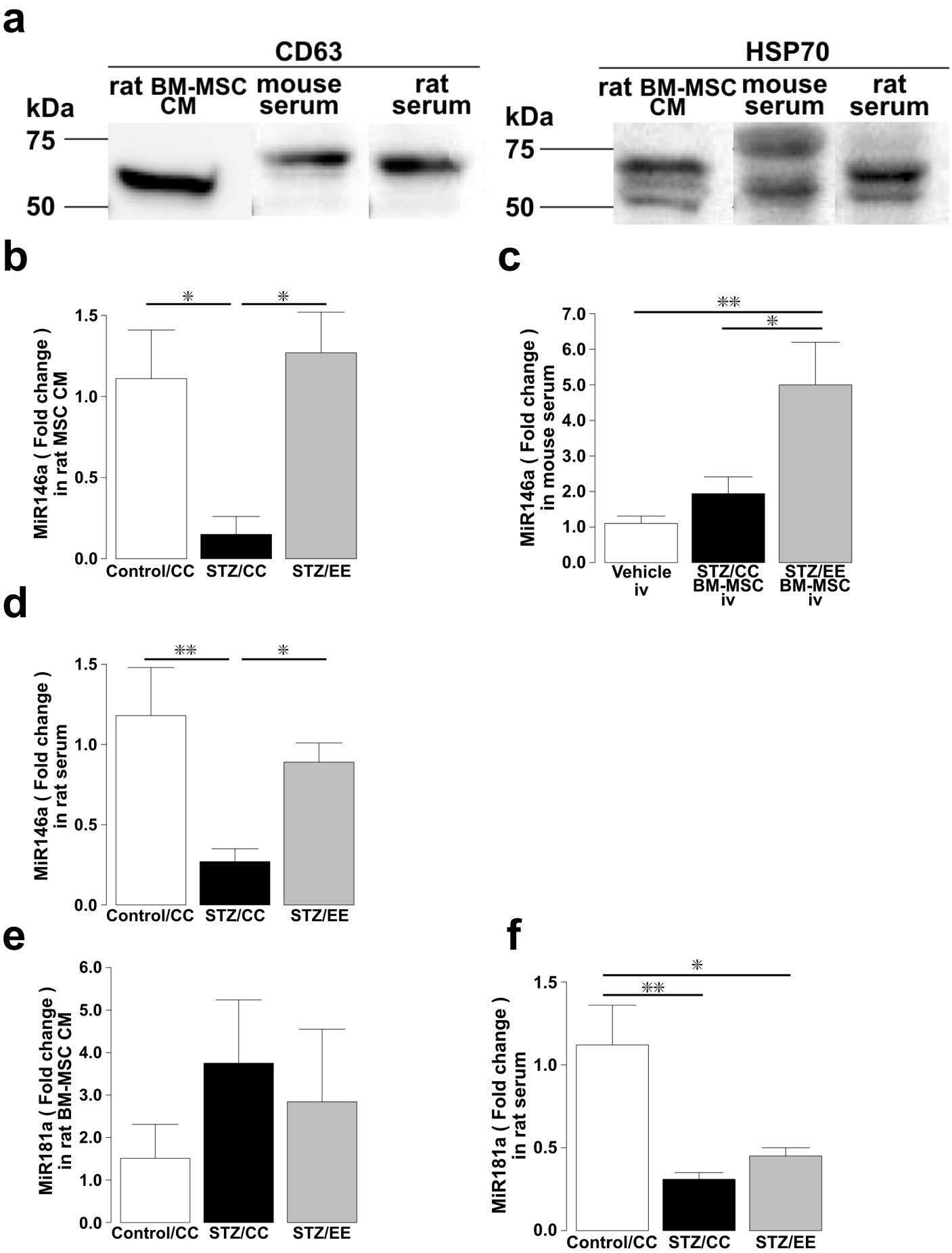
a
CD63
rat BM-MSC CM
mouse serum
rat serum
kDa
75
50
HSP70
rat BM-MSC CM
mouse serum
rat serum
kDa
75
50
b
MiR146a (Fold change) in rat MSC CM
1.5
1.0
0.5
0.0
*
*
Control/CC
STZ/CC
STZ/EE
c
MiR146a (Fold change) in mouse serum
7.0
6.0
5.0
4.0
3.0
2.0
1.0
0.0
**
*
Vehicle iv
STZ/CC BM-MSC iv
STZ/EE BM-MSC iv
d
MiR146a (Fold change) in rat serum
1.5
1.0
0.5
0.0
**
*
Control/CC
STZ/CC
STZ/EE
e
MiR181a (Fold change) in rat BM-MSC CM
6.0
5.0
4.0
3.0
2.0
1.0
0.0
Control/CC
STZ/CC
STZ/EE
f
MiR181a (Fold change) in rat serum
1.5
1.0
0.5
0.0
*
**
Control/CC
STZ/CC
STZ/EE

Supplementary information

1. Supplementary Figure

2. Methods

An enriched environment improves diabetes-induced cognitive impairment by enhancing exosomal miR-146a secretion from endogenous bone marrow-derived mesenchymal stem cells.

Kenta Kubota, Masako Nakano, Eiji Kobayashi, Yuka Mizue, Takako Chikenji, Miho Otani, Kanna Nagaishi, Mineko Fujimiya

Supplementary Figure 1

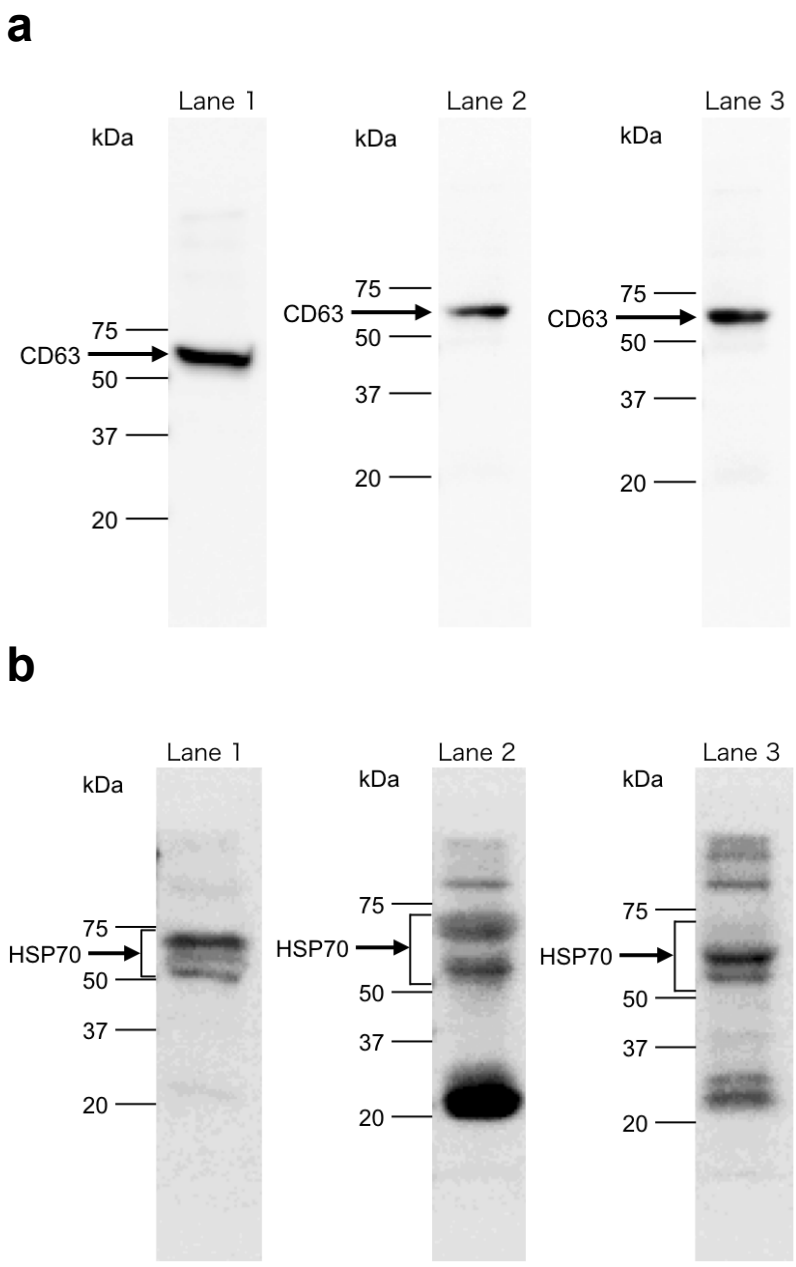

(a) The full-length blots in Figure 6a. CD 63 are detected in exosomes derived from conditional medium of cultured BM-MSC (Lane 1), exosomes derived from rat serum (Lane 2), and exosomes derived from mouse serum (Lane 3). Molecular weight of CD63 is ~53 kDa.

(b) The full-length blots in Figure 6a. HSP70 are detected in exosomes derived from conditional medium of cultured BM-MSC (Lane 1), exosomes derived from rat serum (Lane 2), and exosomes derived from mouse serum (Lane 3). Molecular weight of HSP70 is 53-70 kDa.

Supplementary Methods

Western blot analysis.

The denatured proteins from exosomal pellets were separated on 12% SDS-polyacrylamide gels, and transferred to PVDF membranes. After blocking with 5% skim milk, the membranes were incubated overnight at 4℃ with primary antibodies against CD63 (rabbit polyclonal, 1:1,000, System Biosciences) and HSP70 (rabbit polyclonal, 1:1,000, System Biosciences). After washing, and incubation with secondary HRP-conjugated goat anti-rabbit IgG (1:20,000, System Biosciences) the blots were developed using a Pierce western blotting substrate kit (Thermo Fisher Scientific). Digital images were produced using a Las-3000 imaging system (Fujifilm Life Science, Kanagawa, Japan).